

# Collective Modes in a Superfluid Neutron Gas within the Quasiparticle Random-Phase Approximation

Noël Martin\* and Michael Urban†

*Institut de Physique Nucléaire, CNRS/IN2P3 and Université Paris-Sud 11, F-91406 Orsay Cedex, France*

We study collective excitations in a superfluid neutron gas at zero temperature within the quasiparticle random phase approximation. The particle-hole residual interaction is obtained from a Skyrme functional, while a separable interaction is used in the pairing channel which gives a BCS gap that is very similar to the one obtained with a realistic nucleon-nucleon interaction. In accordance with the Goldstone theorem, we find an ungapped collective mode (analogous to the Bogoliubov-Anderson mode). At low momentum, its dispersion relation is approximately linear and its slope coincides with the hydrodynamic speed of sound calculated with the Skyrme equation of state. The response functions are compared with those obtained within the Landau approximation. We also compute the contribution of the collective mode to the specific heat of the neutron gas.

PACS numbers: 21.65.Cd,03.75.Kk,26.60.Gj

Keywords:

## I. INTRODUCTION

In the inner crust of neutron stars, very neutron-rich nuclei are immersed in a gas of unbound neutrons [1]. A few minutes after the formation of the neutron star, it has already cooled down below the superfluid transition temperature  $T_c$  of the neutron gas, i.e., the neutrons form Cooper pairs. This strongly suppresses the neutron contribution to the specific heat at low temperatures  $T < T_c$  [2]. However, it was pointed out that the contribution of collective modes to the specific heat can be very important [3]. In particular the contribution of acoustic phonons with long wavelengths is dominant over that of gapped neutron quasiparticles at low temperatures [4].

In the present paper we will restrict ourselves to a simplified system, namely a uniform neutron gas. Collective excitations in uniform neutron and nuclear matter have been extensively studied within the random-phase approximation (RPA) [5, 6]. Collectivity may, e.g., strongly affect the neutrino mean-free path [7]. In ordinary RPA, however, pairing between the neutrons is not included. The extension of RPA which accounts for pairing is called the quasiparticle RPA (QRPA). Calculations with pairing in neutron matter [8] and in  $\beta$ -stable neutron-proton-electron (*npe*) matter [9] (as it exists in the neutron-star core) have been performed within the Landau approximation. But it is known from RPA calculations [5] that results obtained within the Landau approximation can differ substantially from those obtained with the full residual particle-hole (ph) interaction derived from the Skyrme functional. One of the goals of the present paper is to perform a full QRPA calculation where the same Skyrme interaction that is used for the description of the ground state is also used as residual interaction among the quasiparticles.

In the pairing channel, we use a separable interaction that is a good approximation to a low-momentum effective interaction ( $V_{\text{low-}k}$ ) obtained by renormalization-group techniques from a realistic nucleon-nucleon force [10]. For the sake of consistency, we use the same interaction in the gap equation and in the particle-particle (pp) channel of the QRPA. This guarantees that the QRPA correctly describes the Bogoliubov-Anderson sound [11, 12], which is a density wave with linear dispersion relation at low momenta. This mode is actually a Goldstone mode [13] related to the broken  $U(1)$  symmetry in the superfluid phase. Note that similar calculations have been performed in other fields of physics, e.g., ultracold atoms [14].

We find that the speed of sound coincides with the hydrodynamic one that can be calculated from the Skyrme equation of state (EOS). We calculate the contribution of the sound mode to the specific heat and find that it is much bigger than that of thermally excited neutron quasiparticles.

The important role of the Goldstone mode in the neutron star crust was already studied in numerous recent papers, e.g. [4, 15–19]. However, in these studies the Goldstone mode was generally treated in the long-wavelength limit and its coupling to the two-quasiparticle continuum was neglected. This coupling, which has already been found to be important, e.g., in the case of ultracold atoms [14, 20], is automatically included in the QRPA.

The paper is organized as follows. In Sec. II, we briefly explain the formalism we use to describe the ground state and the collective modes of neutron matter. In Sec. III, we discuss numerical results, and Sec. IV is devoted to the summary and conclusions. Some technical details are given in the Appendix.

Throughout the article, we use units with  $\hbar = c = k_B = 1$  ( $\hbar$  = reduced Planck constant,  $c$  = speed of light,  $k_B$  = Boltzmann constant).

---

\*Electronic address: noelmartin@ipno.in2p3.fr

†Electronic address: urban@ipno.in2p3.fr

## II. FORMALISM

### A. Skyrme energy density functional

Let us start by briefly summarizing the description of neutron matter using the Skyrme energy-density functional (EDF). The Skyrme functionals [21] have been fitted to a large variety of nuclear data. In addition, in order to be more predictive for neutron-rich nuclei, they have also been fitted to the equation of state of neutron matter [22, 23]. In the case of pure neutron matter, the energy density can be written as

$$\mathcal{E}_{\text{Skyrme}} = \frac{1}{2m}\tau + \frac{s_0}{4}\rho^2 + \frac{s_3}{24}\rho^{\alpha+2} + \frac{s_1 + 3s_2}{8}(\rho\tau - j^2) + 3\frac{s_1 - s_2}{16}(\nabla\rho)^2, \quad (1)$$

with parameters  $s_0, \dots, s_3$  and  $\alpha$  which are defined in Appendix A. In Eq. (1),  $\rho$  denotes the number density of neutrons ( $\rho = \rho_n$ ),  $\tau$  is the kinetic energy density (multiplied by  $2m$ , where  $m$  is the neutron mass), and  $\mathbf{j}$  is the current. In terms of the density matrix

$$\rho_{\mathbf{k},\mathbf{k}'} = \langle a_{\mathbf{k}'\uparrow}^\dagger a_{\mathbf{k}\uparrow} \rangle, \quad (2)$$

where  $a$  and  $a^\dagger$  denote, respectively, neutron annihilation and creation operators, these quantities are defined as

$$\rho(\mathbf{r}) = 2 \sum_{\mathbf{k},\mathbf{k}'} \rho_{\mathbf{k},\mathbf{k}'} e^{i(\mathbf{k}-\mathbf{k}')\cdot\mathbf{r}}, \quad (3a)$$

$$\tau(\mathbf{r}) = 2 \sum_{\mathbf{k},\mathbf{k}'} \mathbf{k} \cdot \mathbf{k}' \rho_{\mathbf{k},\mathbf{k}'} e^{i(\mathbf{k}-\mathbf{k}')\cdot\mathbf{r}}, \quad (3b)$$

$$\mathbf{j}(\mathbf{r}) = \sum_{\mathbf{k},\mathbf{k}'} (\mathbf{k} + \mathbf{k}') \rho_{\mathbf{k},\mathbf{k}'} e^{i(\mathbf{k}-\mathbf{k}')\cdot\mathbf{r}}. \quad (3c)$$

Here we have assumed that the density matrices for both spin projections ( $\uparrow, \downarrow$ ) are equal. The term proportional to  $j^2$  in Eq. (1) is necessary to ensure Galilean invariance [24]. Note that we did not write the spin-orbit interaction since it is absent in spin-unpolarized matter.

In uniform matter, the functional (1) gives rise to a constant Hartree-Fock (HF) potential  $U_{\text{HF}}$  and an effective mass  $m^*$ . The former is the first derivative of Eq. (1) with respect to  $\rho$ , while the effective mass is due to the  $\tau$  dependence of the Skyrme functional [23]:

$$U_{\text{HF}} = \frac{s_0}{2}\rho + \frac{\alpha + 2}{24}s_3\rho^{\alpha+1} + \frac{s_1 + 3s_2}{8}\tau, \quad (4a)$$

$$\frac{1}{2m^*} = \frac{1}{2m} + \frac{s_1 + 3s_2}{8}\rho. \quad (4b)$$

We absorb  $U_{\text{HF}}$  in an effective chemical potential  $\mu^* = \mu - U_{\text{HF}}$ , so that the single-particle spectrum can be written as

$$\xi_{\mathbf{k}} = \epsilon_{\mathbf{k}} - \mu = \frac{k^2}{2m^*} - \mu^*. \quad (5)$$

To study collective excitations within the RPA (or QRPA), one needs the residual interaction between quasi-particles. The corresponding matrix elements in the ph channel are obtained from the Skyrme functional as follows [5]:

$$V_{\mathbf{k}_1, \mathbf{k}_2, \mathbf{k}_4, \mathbf{k}_3}^{\text{ph}} = \frac{\delta^2 E_{\text{Skyrme}}}{\delta\rho_{\mathbf{k}_1, \mathbf{k}_2} \delta\rho_{\mathbf{k}_4, \mathbf{k}_3}}, \quad (6)$$

where  $E_{\text{Skyrme}} = \int d^3r \mathcal{E}_{\text{Skyrme}}$  is the energy. The conservation of the total momentum  $\mathbf{q}$  of the ph pair implies that  $V^{\text{ph}}$  is proportional to  $\delta_{\mathbf{k}_1 - \mathbf{k}_2, \mathbf{k}_3 - \mathbf{k}_4}$ . After transformation to relative and total momenta of the ph pairs, the matrix element can conveniently be written in the form [25]

$$V_{\mathbf{k} + \frac{\mathbf{q}}{2}, \mathbf{k} - \frac{\mathbf{q}}{2}, \mathbf{k}' - \frac{\mathbf{q}'}{2}, \mathbf{k}' + \frac{\mathbf{q}'}{2}}^{\text{ph}} = [W_1(q) + W_2(\mathbf{k} - \mathbf{k}')^2] \delta_{\mathbf{q}, \mathbf{q}'}. \quad (7)$$

The explicit expressions for  $W_1(q)$  and  $W_2$  in terms of the parameters of the Skyrme functional are given in the Appendix A.

### B. Pairing interaction

In order to account for the superfluidity of the neutron gas, we have to include pairing. We do this in the framework of the Bardeen-Cooper-Schrieffer (BCS) theory [26]. Here, we consider only pairing in the  $^1S_0$  channel, i.e., of neutrons with opposite spins, and disregard the  $^3P_2$  channel, which becomes dominant at higher densities [27]. If we define the anomalous density by

$$\kappa_{\mathbf{k}, \mathbf{k}'} = \langle a_{-\mathbf{k}'\downarrow} a_{\mathbf{k}\uparrow} \rangle, \quad (8)$$

the pairing gap  $\Delta$  is given by the gap equation

$$\Delta_{\mathbf{k}_1, \mathbf{k}_2} = - \sum_{\mathbf{k}_3, \mathbf{k}_4} V_{\mathbf{k}_1, \mathbf{k}_2, \mathbf{k}_4, \mathbf{k}_3}^{\text{pp}} \kappa_{\mathbf{k}_3, \mathbf{k}_4}, \quad (9)$$

where  $V_{\mathbf{k}_1, \mathbf{k}_2, \mathbf{k}_4, \mathbf{k}_3}^{\text{pp}}$  is the matrix element of the pairing interaction (for outgoing particles  $\mathbf{k}_1 \uparrow$  and  $-\mathbf{k}_2 \downarrow$ , and incoming particles  $\mathbf{k}_3 \uparrow$  and  $-\mathbf{k}_4 \downarrow$ ).

In nuclear structure calculations with Skyrme interaction, usually a contact interaction with (possibly) density dependent coupling constant and a cut-off is employed (see e.g. [28]). Here, we take a different approach and use a simple separable approximation to a low-momentum interaction ( $V_{\text{low-}k}$ ) derived from a realistic nucleon-nucleon force [10]. This interaction gives a reasonable density dependence of the superfluid critical temperature in low-density neutron matter [29]. The approximation we use is

$$V_{\mathbf{k}_1, \mathbf{k}_2, \mathbf{k}_4, \mathbf{k}_3}^{\text{pp}} = -gF\left(\frac{1}{2}|\mathbf{k}_1 + \mathbf{k}_2|\right) F\left(\frac{1}{2}|\mathbf{k}_3 + \mathbf{k}_4|\right) \times \delta_{\mathbf{k}_1 - \mathbf{k}_2, \mathbf{k}_3 - \mathbf{k}_4}, \quad (10)$$

where  $g$  is the strength of the interaction and  $F$  is a Gaussian form factor

$$F(k) = e^{-k^2/k_0^2}. \quad (11)$$

In the ground state,  $\kappa$  and  $\Delta$  are diagonal, and we define  $\Delta_{\mathbf{k}} = \Delta_{\mathbf{k},\mathbf{k}}$ . Then the gap equation reads

$$\Delta_{\mathbf{k}} = - \sum_{\mathbf{k}'} V_{\mathbf{k},\mathbf{k},\mathbf{k}',\mathbf{k}'}^{pp} \frac{\Delta_{\mathbf{k}'}}{2E_{\mathbf{k}'}} , \quad (12)$$

with the usual quasiparticle energy

$$E_{\mathbf{k}} = \sqrt{\xi_{\mathbf{k}}^2 + \Delta_{\mathbf{k}}^2}. \quad (13)$$

The separable form of the pairing interaction simplifies a lot the solution of the gap equation: it is evident that  $\Delta_{\mathbf{k}}$  is of the form  $\Delta_{\mathbf{k}} = \Delta_0 F(k)$ , and instead of an integral equation for the function  $\Delta_{\mathbf{k}}$  one has to solve only an equation for the number  $\Delta_0$ .

### C. Quasiparticle Random Phase Approximation

The QRPA treats small oscillations around the Hartree-Fock-Bogoliubov (HFB) ground state (which, in the case of uniform matter, is obtained by combining the HF and BCS frameworks discussed in the preceding subsections) [30]. It can be derived by linearising the time dependent HFB (TDHFB) equations, see, e.g., Ref. [28], or, equivalently, by using the formalism of normal and anomalous Green's functions, see, e.g., Refs. [9, 31]. Here we use the TDHFB formalism.

In addition to normal and anomalous density matrices  $\rho$  and  $\kappa$  defined in Eqs. (2) and (8), we define

$$\bar{\rho}_{\mathbf{k},\mathbf{k}'} = \langle a_{-\mathbf{k}\downarrow}^\dagger a_{-\mathbf{k}'\downarrow} \rangle, \quad \kappa_{\mathbf{k},\mathbf{k}'}^\dagger = \langle a_{\mathbf{k}'\uparrow}^\dagger a_{-\mathbf{k}\downarrow}^\dagger \rangle. \quad (14)$$

Then the TDHFB equations can conveniently be written as [30]

$$i\dot{\mathcal{R}} = [\mathcal{H}, \mathcal{R}], \quad (15)$$

with

$$\mathcal{H} = \begin{pmatrix} h & \Delta \\ \Delta^\dagger & -\bar{h} \end{pmatrix}, \quad \mathcal{R} = \begin{pmatrix} \rho & -\kappa \\ -\kappa^\dagger & 1 - \bar{\rho} \end{pmatrix}. \quad (16)$$

The matrices  $h$  and  $\bar{h}$  denote the matrices of the one-body mean-field hamiltonian which will be specified below.

As mentioned before, the QRPA is the linearization of the TDHFB equations for small oscillations around the ground state. We therefore split the matrices  $\mathcal{R}$  and  $\mathcal{H}$  into their ground-state values  $\mathcal{R}^{(0)}$  and  $\mathcal{H}^{(0)}$  and small deviations  $\mathcal{R}^{(1)}$  and  $\mathcal{H}^{(1)}$ . Let us first look at the ground state, which of course has to satisfy Eq. (15) with  $\dot{\mathcal{R}}^{(0)} = 0$ . This is the case because  $\mathcal{H}^{(0)}$  and  $\mathcal{R}^{(0)}$  can be simultaneously diagonalized. In the ground state, we have  $h_{\mathbf{k},\mathbf{k}'}^{(0)} = \bar{h}_{\mathbf{k},\mathbf{k}'}^{(0)} = \xi_{\mathbf{k}} \delta_{\mathbf{k},\mathbf{k}'}$  and  $\Delta_{\mathbf{k},\mathbf{k}'}^{(0)} = \Delta_{\mathbf{k},\mathbf{k}'}^{\dagger(0)} = \Delta_{\mathbf{k}} \delta_{\mathbf{k},\mathbf{k}'}$ ,

and the matrix  $\mathcal{H}^{(0)}$  is diagonalized by the transformation

$$\tilde{\mathcal{H}}^{(0)} = \mathcal{W}^T \mathcal{H}^{(0)} \mathcal{W} = \begin{pmatrix} E & 0 \\ 0 & -E \end{pmatrix}, \quad (17)$$

with the eigenvalues  $E_{\mathbf{k},\mathbf{k}'} = E_{\mathbf{k}} \delta_{\mathbf{k},\mathbf{k}'}$  and the transformation matrix

$$\mathcal{W} = \begin{pmatrix} u & -v \\ v & u \end{pmatrix}, \quad (18)$$

where  $u$  and  $v$  are the usual factors appearing in BCS theory

$$u_{\mathbf{k}} = \sqrt{\frac{1}{2} + \frac{\xi_{\mathbf{k}}}{2E_{\mathbf{k}}}}, \quad v_{\mathbf{k}} = \sqrt{\frac{1}{2} - \frac{\xi_{\mathbf{k}}}{2E_{\mathbf{k}}}}. \quad (19)$$

The normal and anomalous density matrices in the ground state are given by  $\rho_{\mathbf{k},\mathbf{k}'}^{(0)} = \bar{\rho}_{\mathbf{k},\mathbf{k}'}^{(0)} = v_{\mathbf{k}}^2 \delta_{\mathbf{k},\mathbf{k}'}$  and  $\kappa_{\mathbf{k},\mathbf{k}'}^{(0)} = \kappa_{\mathbf{k},\mathbf{k}'}^{\dagger(0)} = u_{\mathbf{k}} v_{\mathbf{k}} \delta_{\mathbf{k},\mathbf{k}'}$ , so that the same transformation diagonalizes  $\mathcal{R}^{(0)}$ , too:

$$\tilde{\mathcal{R}}^{(0)} = \mathcal{W}^T \mathcal{R}^{(0)} \mathcal{W} = \begin{pmatrix} 0 & 0 \\ 0 & 1 \end{pmatrix}. \quad (20)$$

Let us now consider a small perturbation of the system. By keeping in Eq. (15) only the first order in the deviations, we obtain the linearized equation of motion

$$i\dot{\mathcal{R}}^{(1)} = [\mathcal{H}^{(0)}, \mathcal{R}^{(1)}] + [\mathcal{H}^{(1)}, \mathcal{R}^{(0)}]. \quad (21)$$

The equation can be simplified by applying again the transformation that diagonalizes  $\mathcal{H}^{(0)}$  and  $\mathcal{R}^{(0)}$ . After a Fourier transform with respect to time one obtains the following equation:

$$\omega \tilde{\mathcal{R}}^{(1)} = \begin{pmatrix} [E, \tilde{\mathcal{R}}_{11}^{(1)}] & \{E, \tilde{\mathcal{R}}_{12}^{(1)}\} + \tilde{\mathcal{H}}_{12}^{(1)} \\ -\{E, \tilde{\mathcal{R}}_{21}^{(1)}\} - \tilde{\mathcal{H}}_{21}^{(1)} & -[E, \tilde{\mathcal{R}}_{22}^{(1)}] \end{pmatrix}, \quad (22)$$

from which one can easily determine the non-vanishing elements  $\tilde{\mathcal{R}}_{12}^{(1)}$  and  $\tilde{\mathcal{R}}_{21}^{(1)}$  as functions of  $\tilde{\mathcal{H}}_{12}^{(1)}$  and  $\tilde{\mathcal{H}}_{21}^{(1)}$ . The matrix  $\mathcal{R}^{(1)}$  is then obtained by transforming  $\tilde{\mathcal{R}}^{(1)}$  back. The resulting expressions are lengthy, but they can be simplified by using the following linear combinations:

$$\rho^\pm = \rho \pm \bar{\rho}, \quad \kappa^\pm = \kappa \pm \kappa^\dagger, \quad (23)$$

$$h^\pm = h \pm \bar{h}, \quad \Delta^\pm = \Delta \pm \Delta^\dagger. \quad (24)$$

In the case of spin-independent excitations studied in the present paper,  $\rho^+$  is responsible for density oscillations, while  $\rho^-$  describes the corresponding current. (In the case of spin modes, the situation would be reversed.) The quantities  $\kappa^+$  and  $\Delta^+$  are related to oscillations of the amplitude of  $\Delta$ , while  $\kappa^-$  and  $\Delta^-$  describe phase oscillations which are extremely important in the context of the low-energy collective mode (Goldstone mode). The

solution for  $\rho^{\pm(1)}$  and  $\kappa^{\pm(1)}$  can be written in the form

$$\begin{pmatrix} \rho_{\mathbf{k}_1, \mathbf{k}_2}^{+(1)} \\ \rho_{\mathbf{k}_1, \mathbf{k}_2}^{- (1)} \\ \kappa_{\mathbf{k}_1, \mathbf{k}_2}^{+(1)} \\ \kappa_{\mathbf{k}_1, \mathbf{k}_2}^{- (1)} \end{pmatrix} = \Pi_{\mathbf{k}_1, \mathbf{k}_2}^{(0)}(\omega) \begin{pmatrix} h_{\mathbf{k}_1, \mathbf{k}_2}^{+(1)} \\ h_{\mathbf{k}_1, \mathbf{k}_2}^{- (1)} \\ \Delta_{\mathbf{k}_1, \mathbf{k}_2}^{+(1)} \\ \Delta_{\mathbf{k}_1, \mathbf{k}_2}^{- (1)} \end{pmatrix} \quad (25)$$

where  $\Pi_{\mathbf{k}_1, \mathbf{k}_2}^{(0)}(\omega)$  is a  $4 \times 4$  matrix whose components denoted by  $\Pi_{\mathbf{k}_1, \mathbf{k}_2}^{\rho^+, h^+}, \dots, \Pi_{\mathbf{k}_1, \mathbf{k}_2}^{\kappa^-, \Delta^-}$  are given in Appendix B.

So far, we have not specified the perturbation of the hamiltonian,  $h^{(1)}$ . There are two contributions of different origin. First, to probe the system, we apply an external perturbation at  $t = 0$  of the form of a plane wave, i.e.,  $V_{\text{ex}} e^{i\mathbf{q}\cdot\mathbf{r}} \delta(t)$ , which after Fourier transformation becomes  $V_{\text{ex}} \delta_{\mathbf{k}_1 - \mathbf{k}_2, \mathbf{q}}$ . The second contribution to  $h^{(1)}$  comes from the oscillations of the mean field due to the density oscillations :

$$h_{\mathbf{k}_1, \mathbf{k}_2}^{(1)} = V_{\text{ex}} \delta_{\mathbf{k}_1 - \mathbf{k}_2, \mathbf{q}} + \sum_{\mathbf{k}_3, \mathbf{k}_4} V_{\mathbf{k}_1, \mathbf{k}_2, \mathbf{k}_4, \mathbf{k}_3}^{\text{ph}} \rho_{\mathbf{k}_3, \mathbf{k}_4}^{(1)}. \quad (26)$$

Analogously, the oscillation of the gap,  $\Delta^{(1)}$ , is related to the oscillation of the anomalous density,

$$\Delta_{\mathbf{k}_1, \mathbf{k}_2}^{(1)} = - \sum_{\mathbf{k}_3, \mathbf{k}_4} V_{\mathbf{k}_1, \mathbf{k}_2, \mathbf{k}_4, \mathbf{k}_3}^{\text{pp}} \kappa_{\mathbf{k}_3, \mathbf{k}_4}^{(1)}. \quad (27)$$

Looking at Eq. (25) and taking into account the momentum conservation in the interactions  $V^{\text{ph}}$  and  $V^{\text{pp}}$ , one sees that an external perturbation proportional to  $\delta_{\mathbf{k}_1 - \mathbf{k}_2, \mathbf{q}}$  leads to non-vanishing elements of  $\rho_{\mathbf{k}_1, \mathbf{k}_2}$  and  $\kappa_{\mathbf{k}_1, \mathbf{k}_2}$  only for  $\mathbf{k}_1 - \mathbf{k}_2 = \mathbf{q}$ . This could have been anticipated, since in a uniform system a perturbation having the form of a plane wave can only excite oscillations which are also plane waves with the same wave vector as the perturbation. We therefore introduce the short-hand notation  $\mathbf{k}_{\pm} = \mathbf{k} \pm \frac{\mathbf{q}}{2}$  and denote the non-vanishing matrix elements by  $\rho_{\mathbf{k}_+, \mathbf{k}_-}$ , etc.

The advantage of the Skyrme functional is that  $h^{(1)}$  depends only on local quantities. With the notation of Eq. (7), we have

$$h_{\mathbf{k}_+, \mathbf{k}_-}^{+(1)} = W_1(q) \rho_{\mathbf{q}}^{+(1)} + W_2 k^2 \rho_{\mathbf{q}}^{+(1)} + W_2 \tau_{\mathbf{q}}^{+(1)} + 2V_{\text{ex}}, \quad (28a)$$

$$h_{\mathbf{k}_+, \mathbf{k}_-}^{- (1)} = 2W_2 k \cos \theta j_{\mathbf{q}}^{- (1)}, \quad (28b)$$

where  $\theta$  is the angle between  $\mathbf{k}$  and  $\mathbf{q}$  and

$$\rho_{\mathbf{q}}^{+(1)} = \sum_{\mathbf{k}} \rho_{\mathbf{k}_+, \mathbf{k}_-}^{+(1)}, \quad (29a)$$

$$\tau_{\mathbf{q}}^{+(1)} = \sum_{\mathbf{k}} k^2 \rho_{\mathbf{k}_+, \mathbf{k}_-}^{+(1)}, \quad (29b)$$

$$j_{\mathbf{q}}^{- (1)} = \sum_{\mathbf{k}} k \cos \theta \rho_{\mathbf{k}_+, \mathbf{k}_-}^{- (1)}. \quad (29c)$$

Similarly, in the pp channel, the calculation is simplified by the fact that our pairing interaction (10) is separable:

$$\Delta_{\mathbf{k}_+, \mathbf{k}_-}^{\pm(1)} = g F(k) \kappa_{\mathbf{q}}^{\pm(1)} \quad (30)$$

with

$$\kappa_{\mathbf{q}}^{\pm(1)} = \sum_{\mathbf{k}} F(k) \kappa_{\mathbf{k}_+, \mathbf{k}_-}^{\pm(1)} \quad (31)$$

Now we are able to calculate the linear response by inserting Eqs. (25), (28) and (30) into Eqs. (29) and (31). In this way we obtain

$$\begin{pmatrix} \rho_{\mathbf{q}}^{+(1)} \\ \tau_{\mathbf{q}}^{+(1)} \\ j_{\mathbf{q}}^{- (1)} \\ \kappa_{\mathbf{q}}^{+(1)} \\ \kappa_{\mathbf{q}}^{- (1)} \end{pmatrix} = \left( \mathbb{I} - \langle\langle \Pi_{\mathbf{q}}^{(0)} V \rangle\rangle \right)^{-1} \begin{pmatrix} \langle\langle \Pi_{\mathbf{k}_+, \mathbf{k}_-}^{\rho^+, h^+} \rangle\rangle \\ \langle\langle k^2 \Pi_{\mathbf{k}_+, \mathbf{k}_-}^{\rho^+, h^+} \rangle\rangle \\ \langle\langle k \cos \theta \Pi_{\mathbf{k}_+, \mathbf{k}_-}^{\rho^-, h^+} \rangle\rangle \\ \langle\langle F(k) \Pi_{\mathbf{k}_+, \mathbf{k}_-}^{\kappa^+, h^+} \rangle\rangle \\ \langle\langle F(k) \Pi_{\mathbf{k}_+, \mathbf{k}_-}^{\kappa^-, h^+} \rangle\rangle \end{pmatrix} 2V_{\text{ex}}, \quad (32)$$

where the short-hand notation  $\langle\langle f(\mathbf{k}) \rangle\rangle$  denotes the sum of  $f(\mathbf{k})$  over  $\mathbf{k}$ ,

$$\langle\langle f(\mathbf{k}) \rangle\rangle = \sum_{\mathbf{k}} f(\mathbf{k}), \quad (33)$$

and the matrix  $\langle\langle \Pi_{\mathbf{q}}^{(0)} V \rangle\rangle$  is given in Appendix B.

It is well known that superfluidity leads to the existence of the so-called Bogoliubov-Anderson sound [11, 12], a collective mode with linear dispersion relation  $\omega \propto q$  (for small  $q$ ) which can be interpreted as a Goldstone boson corresponding to the broken U(1) symmetry [32]. This implies that the QRPA response function has a pole at low energy. The energy  $\omega$  of this collective mode can be found by searching for a given  $q$  the root of the determinant of the matrix appearing in Eq. (32):

$$\left| \mathbb{I} - \langle\langle \Pi_{\mathbf{q}}^{(0)} V \rangle\rangle \right| = 0. \quad (34)$$

This collective mode exists only at low momentum  $q$ , as long as its energy  $\omega$  lies below the pair-breaking threshold  $\sim 2\Delta_{k_F}$ , where  $k_F$  denotes the Fermi momentum. At higher values of  $q$ , the collective mode enters the two-quasiparticle continuum and gets a width (finite lifetime).

#### D. Landau approximation

In some recent work [8, 9], the QRPA response was calculated within the Landau approximation [33]. In this approximation, one exploits the fact that for small  $q$  the change of the density matrix  $\rho_{\mathbf{k}, \mathbf{k}'}$  is concentrated at the Fermi surface,  $|\mathbf{k}| \approx |\mathbf{k}'| \approx k_F$ . Keeping only the Landau parameter  $F_0$  amounts to replacing Eq. (28) by

$$h_{\mathbf{k}_+, \mathbf{k}_-}^{+(1)} = (W_1(0) + 2W_2 k_F^2) \rho_{\mathbf{q}}^{+(1)} \quad (35)$$

and neglecting  $h_{\mathbf{k}_+, \mathbf{k}_-}^{-(1)}$ . However, because of the effective mass  $m^* \neq m$ , this approximation violates Galilean invariance [33] and one should also include the parameter  $F_1$ . In this case one has

$$h_{\mathbf{k}_+, \mathbf{k}_-}^{-(1)} = 2W_2 k_F \cos \theta j_{\mathbf{q}}^{-(1)}, \quad (36)$$

where the current  $j_{\mathbf{q}}^{-(1)}$  is calculated from

$$j_{\mathbf{q}}^{-(1)} = k_F \sum_{\mathbf{k}} \cos \theta \rho_{\mathbf{k}_+, \mathbf{k}_-}^{-(1)}. \quad (37)$$

As a consequence, the  $5 \times 5$  matrix in Eq. (32) reduces to a  $3 \times 3$  or  $4 \times 4$  one if one keeps only  $F_0$  or  $F_0$  and  $F_1$ , respectively.

### E. Hydrodynamics

The famous result for the dispersion relation of the Bogoliubov-Anderson mode,  $\omega = k_F q / (\sqrt{3}m)$ , first derived by Bogoliubov [11] and Anderson [12], would be correct in an ideal Fermi gas. Leggett [34] generalized this result in the framework of Landau's Fermi-liquid theory to include the interaction among quasiparticles. In both cases the sound velocity  $u = \omega/q$  agrees with the hydrodynamic one,

$$u^2 = \frac{1}{m\rho} \left. \frac{\partial P}{\partial \rho} \right|_s \quad (38)$$

( $P$  and  $s$  are the pressure and the entropy density, respectively), which in the zero-temperature case can be simplified to

$$u^2 = \frac{1}{m} \left. \frac{\partial \mu}{\partial \rho} \right|_{T=0}, \quad (39)$$

since  $s = 0$  at  $T = 0$ .

At a first glance, it is surprising that hydrodynamics is applicable here. In a normal fluid, hydrodynamics requires collisions that restore local equilibrium. Otherwise, in the collisionless regime, the local Fermi sphere gets deformed during the oscillation, which gives rise to the so-called zero-sound modes [33]. The situation is completely different in a superfluid at  $T = 0$ : although there are no collisions, the local Fermi sphere stays spherical during the oscillation because of pairing. This ‘‘superfluid hydrodynamics’’ was also used to describe collective modes in trapped (i.e., non-uniform) Fermi gases [35], and in Ref. [36] it was demonstrated that also in that case hydrodynamic and QRPA results for  $T = 0$  agree if pairing is strong enough.

In order to calculate the hydrodynamic speed of sound, we use in Eq. (39) the chemical potential obtained with the Skyrme functional (with pairing).

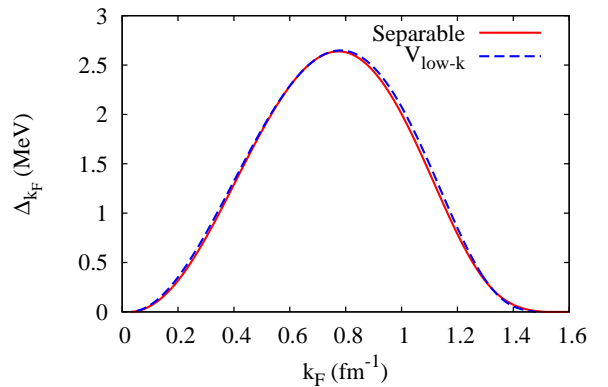


FIG. 1: (Color online) Value of the gap at the Fermi surface,  $\Delta_{k_F}$ , as function of the Fermi momentum  $k_F$ , obtained with the separable interaction (solid line) and with the  $V_{\text{low-}k}$  interaction of [10] (dashes).

TABLE I: Parameters of the pairing interaction, Eqs. (10) and (11).

$g$ (MeV fm <sup>3</sup> )	856
$k_0$ (fm <sup>-1</sup> )	1.367

## III. RESULTS

### A. Ground state

Before we turn to the linear response, let us briefly discuss the ground state properties. For the mean field, we use the SLy4 parametrization of the Skyrme force, whose parameters are given in Ref. [23]. This interaction was not only fitted to nuclei, but also to the EOS of neutron matter. Since pairing has only a marginal effect on the EOS, our EOS agrees with that shown, e.g., in Ref. [37].

To determine the two parameters  $g$  and  $k_0$  of our pairing interaction, Eqs. (10) and (11), we first solve the gap equation (12) with the (non-separable)  $V_{\text{low-}k}$  interaction<sup>1</sup>. The resulting gap at the Fermi surface,  $\Delta_{k_F}$ , as a function of  $k_F = (3\pi^2\rho)^{1/3}$ , is displayed in Fig. 1 (dashes). Then we fit  $g$  and  $k_0$  to reproduce this result with the separable interaction. The result of this fit is also shown in Fig. 1 (solid line), and the corresponding parameter values are listed in Table I. We see that with this pairing interaction, the maximum of the gap,  $\Delta_{k_F} \sim 2.7$  MeV, is reached at  $k_F \sim 0.8$  fm<sup>-1</sup>, corresponding to a density of  $\rho \sim 0.017$  fm<sup>-3</sup>. At low density, the gap increases with density because of the increasing

<sup>1</sup> The matrix elements used here are those obtained in Ref. [10] with a Fermi-Dirac regulator with  $\Lambda = 2$  fm<sup>-1</sup> and  $\epsilon = 0.5$  fm<sup>-1</sup>.

level density at the Fermi surface. The decrease of the gap at high density is due to the form factor, Eq. (11), and not due to an explicit density dependence of the pairing interaction as it is often used in HFB and QRPA calculations with Skyrme forces (see, e.g., Ref. [28]). The fact that our maximum gap is reduced by  $\sim 10\%$  compared to typical BCS results obtained with the free nucleon mass [38] is a consequence of the reduction of the density of states due to the effective mass  $m^* < m$ .

However, it should be pointed out that there is no consensus in the literature about the correct density dependence of the gap [39, 40], mainly because of screening effects beyond BCS theory (analogous to the Gorkov–Melik-Barkhudarov correction [41]), which could lead to a dramatic suppression of the gap. At low density, recent Quantum-Monte-Carlo calculations [42, 43] seem to be reliable and show a suppression of the gap between 30 and 50% compared to the BCS result.

## B. QRPA response function and collective mode

We will now study the QRPA response function in neutron matter for different densities and compare it with the RPA one. In the present work we consider the density response, which is defined by  $\Pi(\omega, q) = \rho_{\mathbf{q}}^{+(1)}/(2V_{\text{ex}})$ . Since its real and imaginary parts are related to each other via dispersion relations, it is enough to discuss the imaginary part, the so-called strength function.

We choose densities between  $0.016$  and  $0.04 \text{ fm}^{-3}$ , corresponding to typical densities of the neutron gas surrounding the clusters in the inner crust of a neutron star [1]. At higher densities, as they are realized in the neutron star core, our approach is not valid because there the neutrons are paired in the  ${}^3P_2$  channel [27]. As we have seen in the preceding subsection, the  ${}^1S_0$  gap decreases with increasing density. We therefore expect that at high density, our QRPA response approaches the RPA one. The latter is the response calculated without pairing, i.e., by setting  $\Delta_{\mathbf{k}} = 0$  and keeping only the upper left  $3 \times 3$  part of the matrix in Eq. (32), and we checked that it coincides with the RPA response functions that can be found in the literature [5]. As one can see in Fig. 2, where the strength function is shown for  $\rho = 0.04 \text{ fm}^{-3}$ , the RPA (dashes) and QRPA (solid lines) responses are indeed similar and approach each other with increasing excitation energy  $\omega$  and momentum transfer  $q$ . For  $q = k_F$  (upper panel) and  $2k_F$  (lower panel), the RPA strength function has a broad continuum. The effect of pairing is to shift the threshold of the continuum from zero to the pair-breaking threshold  $\sim 2\Delta_{k_F}$ . At excitation energies much larger than  $2\Delta_{k_F}$ , the response is practically not affected by pairing. At energies around the threshold, however, the response is strongly modified by pairing. The peak visible at the threshold corresponds to a collective mode which is damped since it lies in the continuum, i.e., it can decay into two quasiparticles. In RPA, one does not see any collective mode, since the ph inter-

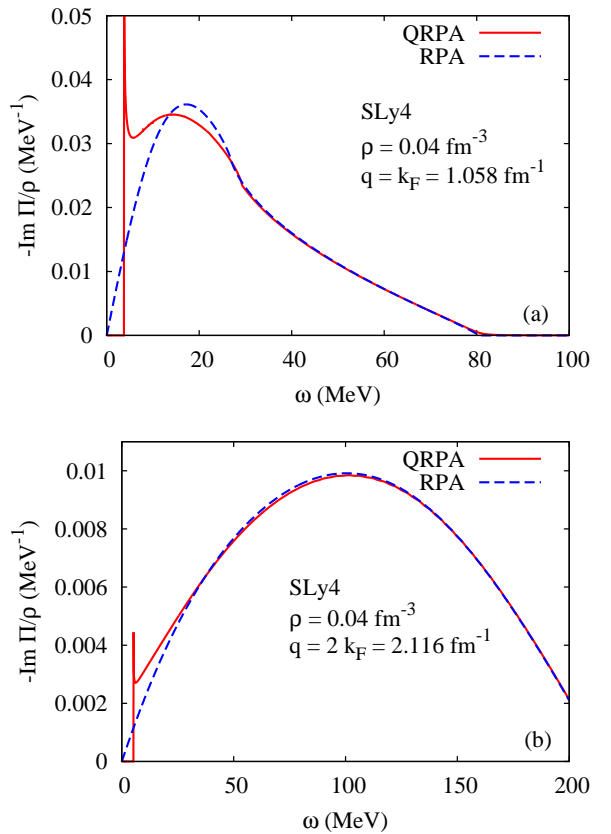


FIG. 2: (Color online) QRPA (solid lines) and RPA (dashes) response functions at density  $\rho = 0.04 \text{ fm}^{-3}$ , as functions of the excitation energy  $\omega$  for two different momentum transfers  $q = k_F$  (a) and  $2k_F$  (b).

action is attractive and a collective zero-sound mode, as it can be described by RPA, exists only for repulsive ph interaction [33].

In the preceding examples the collective mode was damped because we considered a high momentum  $q$  and relatively weak pairing. In order to see more clearly the collective mode, let us now choose a lower density  $\rho = 0.016 \text{ fm}^{-3}$  and smaller momenta. In the upper panel of Fig. 3, we see the imaginary part of the response function for momenta between  $q = 0.5 k_F$  and  $1.3 k_F$ . Now there is a pole in the real part of the response function below the continuum threshold, corresponding to an undamped collective mode. In principle, the imaginary part has a  $\delta$ -function peak at this energy, which is represented as an arrow in Fig. 3. The height of each arrow indicates the strength contained in the peak, which is proportional to the derivative  $d(\Pi^{-1})/d\omega$  calculated at the pole of  $\Pi$ . We can see that the strength is highest for small  $q$  and decreases as the mode approaches the continuum threshold. At momenta higher than  $\sim 1.5 \text{ fm}^{-1}$  (see lower panel of Fig. 3), the collective mode enters again into the continuum, as in Fig. 2.

Let us study in more detail the dispersion relation  $\omega_{\mathbf{q}}$

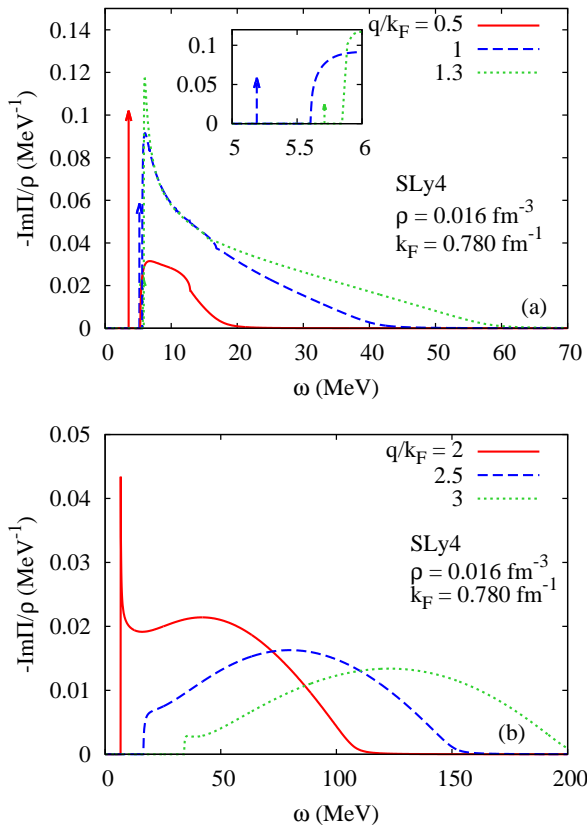


FIG. 3: (Color online) QRPA response functions for  $q/k_F = 0.5, 1, 1.3$  (a) and  $2, 2.5, 3$  (b) at  $\rho = 0.016 \text{ fm}^{-3}$  as functions of the excitation energy  $\omega$ . The arrows in the upper panel represent  $\delta$ -function peaks corresponding to the undamped collective modes. Their height is proportional to their strength which corresponds to 71.3% ( $q = 0.5 k_F$ ), 25.2% ( $q = k_F$ ), and 9.5% ( $q = 1.3 k_F$ ) of the total strength of the response function. In the lower panel (b), the collective mode lies above the continuum threshold.

of the collective mode. In Fig. 4, the solid lines represent the dispersion relations of the undamped collective mode at densities  $\rho = 0.016$  (upper panel) and  $0.04 \text{ fm}^{-3}$  (lower panel). We see that at small  $q$ , the dispersion relation is practically linear. The fact that  $\omega \rightarrow 0$  for  $q \rightarrow 0$ , as required by the Goldstone theorem, is in practice a very good test of our numerics, since  $\omega_{\mathbf{q}=0}$  is extremely sensitive to small numerical errors in the matrix  $\langle\langle \Pi_{\mathbf{q}}^{(0)} V \rangle\rangle$ . Another test is the slope  $d\omega/dq$  at  $q = 0$ , which agrees perfectly with the hydrodynamic speed of sound calculated from Eq. (39) (dash-dotted lines). We see that  $\omega_{\mathbf{q}}$  stays more or less linear as long as  $\omega \ll 2\Delta_{k_F}$ . Since in the case  $\rho = 0.04 \text{ fm}^{-3}$  the gap  $\Delta_{k_F}$  is smaller and the speed of sound  $u$  is higher, the range of applicability of the hydrodynamic approximation is smaller than in the case  $\rho = 0.016 \text{ fm}^{-3}$ . At larger  $q$ , the mode frequency starts to bend and approaches the pair-breaking threshold, which is represented by the dots (approaching  $2\Delta_{k_F}$  and  $q(q/2 - k_F)/m^*$ , respectively, in the limits

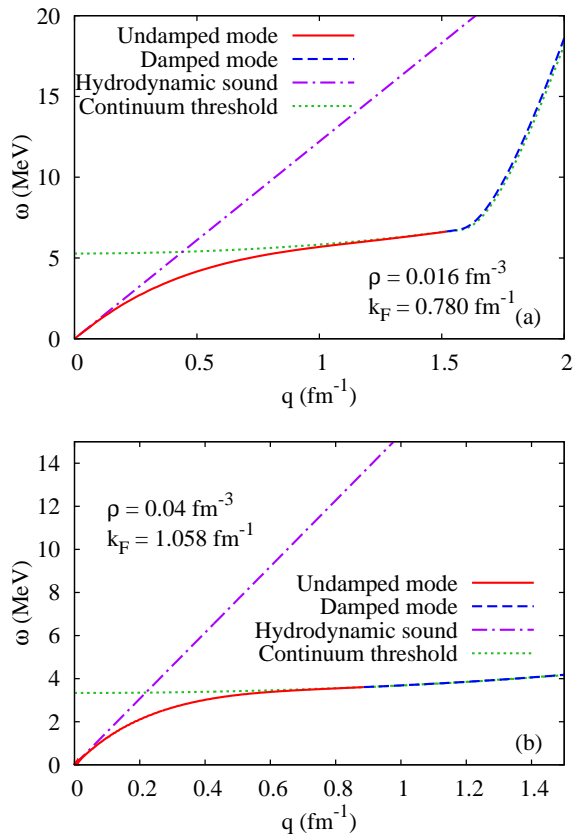


FIG. 4: (Color online) Dispersion relation  $\omega_{\mathbf{q}}$  of the undamped (solid line) and damped (dashes) collective mode at  $\rho = 0.016$  (a) and  $0.04 \text{ fm}^{-3}$  (b). At small  $q$ , it agrees with the linear dispersion relation  $\omega = uq$  of hydrodynamic sound (dash-dotted line). At higher  $q$ , it approaches and finally crosses the pair-breaking threshold (dotted line).

of very small and very large  $q/k_F$ ). Above a certain  $q$ , (e.g.,  $\sim 1.5 \text{ fm}^{-1}$  for  $\rho = 0.016 \text{ fm}^{-3}$  and  $\sim 0.9 \text{ fm}^{-1}$  for  $\rho = 0.04 \text{ fm}^{-3}$ ) the mode enters into the continuum (dashes) but it stays practically at the threshold (cf. also lower panel of Fig. 3). This behavior of the collective mode is qualitatively different from the one shown in Ref. [8] but similar to the one obtained in Ref. [9]. Also in the context of ultracold atoms, results similar to ours have been found, see Ref. [14] for a QRPA calculation and Ref. [20] where the collective mode was studied as small-amplitude oscillation in a time-dependent density-functional theory implementation (similar to TDHFB).

### C. Comparison with the Landau approximation

Now we discuss the results obtained within the Landau approximation as explained in Sec. IID. This approximation has recently been used in Refs. [8, 9]. In Fig. 5 we display response functions for two different densities ( $\rho = 0.016$  and  $0.04 \text{ fm}^{-3}$ ) and momenta ( $q = 0.3$  and  $1.5 \text{ fm}^{-1}$ ) within the Landau approximation keeping only

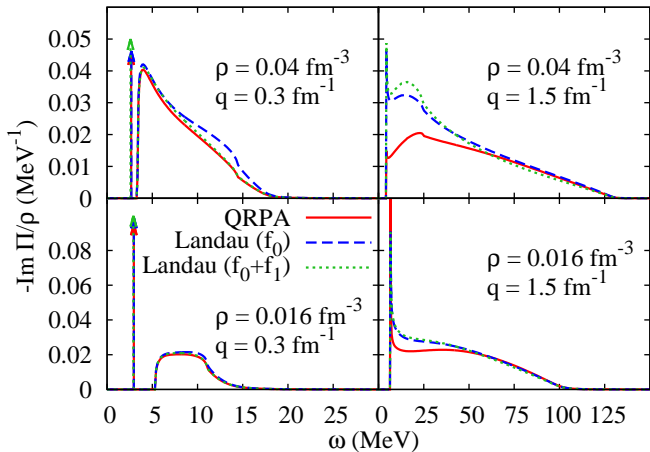


FIG. 5: (Color online) Response functions obtained within the full QRPA (solid lines) and within the Landau approximation including only  $F_0$  (dotted lines) or  $F_0$  and  $F_1$  (dashes) as functions of the excitation energy  $\omega$  for neutron densities  $\rho = 0.016 \text{ fm}^{-3}$  (lower panels) and  $0.04 \text{ fm}^{-3}$  (upper panels) and momenta  $q = 0.3 \text{ fm}^{-1}$  (left panels) and  $1.5 \text{ fm}^{-1}$  (right panels). The arrows in the left panels indicate positions and strengths of the collective modes. In QRPA, the strengths of the collective modes correspond to 82% ( $\rho = 0.016 \text{ fm}^{-3}$ ) and 52% ( $\rho = 0.04 \text{ fm}^{-3}$ ) of the total strength of the response functions.

$F_0$  (dotted lines), and within the Landau approximation keeping  $F_0$  and  $F_1$  as required by Galilean invariance (dashes), and compare them with the full QRPA results (solid lines). In the case of small momentum transfer ( $q = 0.3 \text{ fm}^{-1}$ , left panels of Fig. 5), the three calculations give very similar results. As in Fig. 3, the arrows indicate the energy and strength of the undamped collective mode. We see that the Landau approximation (with  $F_0$  and  $F_1$ , and even with  $F_0$  only) works very well for the energy of the collective mode, only the strength (height of the arrow) is slightly different from that obtained in the full QRPA<sup>2</sup>. At excitation energies above  $\sim 10 \text{ MeV}$  one starts to see a difference between the two Landau approximations. As expected, the result obtained with  $F_0$  and  $F_1$  is in better agreement with the full QRPA than that obtained with  $F_0$  only, as one can see in the upper left panel of Fig. 5.

The situation is completely different at higher momentum transfer. In the right panels of Fig. 5, we show results for  $q = 1.5 \text{ fm}^{-1}$ . In this case, the collective mode has disappeared in the continuum. Now the responses

obtained within the Landau approximation and within the full QRPA are clearly different. This is not surprising, since the basic assumption underlying the Landau approximation, namely that the excited quasiparticles are close to the Fermi surface, is no longer fulfilled, and also the  $q$  dependence of the residual ph interaction [term  $W_1(q)$ ] is no longer negligible. We note that the inclusion of the  $F_1$  Landau parameter does not improve the agreement of the Landau approximation with the full QRPA in this case.

To conclude, the Landau approximation seems to be sufficient to establish the dispersion curve of the collective mode of the neutron gas. However, it may strongly affect calculations that need the entire response function, e.g. the neutrino mean free path in neutron stars [7].

#### D. Heat capacity

In Ref. [2] it was pointed out that neutron pairing results in a strong suppression of the heat capacity at low temperature, which might have observable effects on the neutron star cooling. The relevant temperature range is  $T \lesssim 10^9 \text{ K} \sim 100 \text{ keV}$ , which is much smaller than  $\Delta_{k_F}$  in the region we are interested in. The quasiparticle contribution to the specific heat at temperature  $T$  can be obtained from

$$c_{v,\text{qp}} = T \left. \frac{\partial s_{\text{qp}}}{\partial T} \right|_{\rho}, \quad (40)$$

where  $s_{\text{qp}}$  denotes the entropy density of thermally excited quasiparticles [44]

$$s_{\text{qp}} = -2 \sum_{\mathbf{p}} \left[ (1 - f(E_{\mathbf{p}})) \ln(1 - f(E_{\mathbf{p}})) + f(E_{\mathbf{p}}) \ln(f(E_{\mathbf{p}})) \right] \quad (41)$$

with  $f(E) = 1/(e^{E/T} + 1)$ . Indeed,  $c_{v,\text{qp}}$  is suppressed by a factor of  $e^{-\Delta_{k_F}/T}$  at low temperature, as it is the case in superconducting metals [45]. Note that in a superconductor, the Bogoliubov-Anderson mode is shifted upwards to the plasma frequency by the Coulomb interaction [46] and therefore its contribution to the specific heat is negligible. However, in a superfluid such as the neutron gas the situation is different because here the Bogoliubov-Anderson mode is the dominant contribution to the specific heat at low temperature, and not the quasiparticles.

At  $T \ll \Delta_{k_F}$ , we can neglect the temperature dependence of the collective mode itself, i.e., we can calculate its contribution to the specific heat by using its dispersion relation  $\omega_{\mathbf{q}}$  obtained at  $T = 0$ :

$$c_{v,\text{coll}} = \frac{1}{T^2} \sum_{\mathbf{q}} \frac{\omega_{\mathbf{q}}^2 e^{\omega_{\mathbf{q}}/T}}{(e^{\omega_{\mathbf{q}}/T} - 1)^2}. \quad (42)$$

<sup>2</sup> It is well known that the sound velocity is given by  $u^2 = k_F^2 / (3m^*(1 + F_0)(1 + F_1/3))$  [34]. However, the last term depending on  $F_1$  does not originate from the residual interaction, but from the effective mass  $m^*$ , which is related to  $F_1$  by Galilean invariance:  $u^2 = k_F^2 / (3mm^*(1 + F_0))$  [33]. Therefore, if one calculates the response function with the effective mass  $m^*$ , one already obtains the correct sound velocity by including only  $F_0$  in the residual interaction.



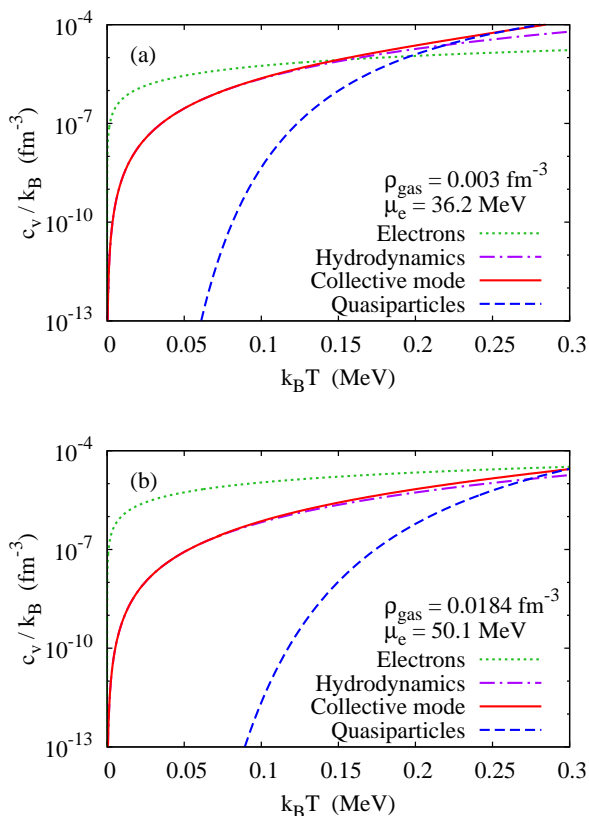


FIG. 6: (Color online) Heat capacity of a neutron gas with density  $\rho = 0.003$  (a) and  $0.0184 \text{ fm}^{-3}$  (b), corresponding to total baryon densities in the neutron-star crust of  $\rho_B \approx 0.00373$  and  $0.0204 \text{ fm}^{-3}$ , respectively: neutron quasiparticle contribution (dashes), contribution of the collective mode calculated within QRPA (solid lines) and within the hydrodynamic approximation (dashed-dotted lines). For comparison, we also display the electron contribution (dotted lines) under the assumption of  $\mu_e = 36.2$  (a) and  $50.1 \text{ MeV}$  (b), corresponding to electron densities  $\rho_e = 2.1 \cdot 10^{-4}$  and  $5.5 \cdot 10^{-4} \text{ fm}^{-3}$ .

At low temperatures, this reduces to

$$c_{v,\text{coll}} = \frac{2\pi^2 T^3}{15u^3}, \quad (43)$$

where  $u$  is the sound velocity of the collective mode. The  $T^3$  behavior is analogous to the specific heat of phonons in a solid [47, 48]. So, we see that at low temperatures the contribution of the neutron gas to the specific heat is reduced as compared to the specific heat of unpaired neutrons, which would be linear in  $T$ . But the reduction is not as drastic as the exponential suppression of  $c_{v,\text{qp}}$ . This is illustrated in Fig. 6, where the specific heats of the quasiparticles, Eq. (40) (dashed lines), and of the collective mode, Eq. (42) (solid lines), are displayed as functions of temperature. As densities of the neutron gas we take  $\rho = 0.003$  (upper panel) and  $0.0184 \text{ fm}^{-3}$  (lower panel), which appear in the neutron-star crust at

total baryon densities of  $\rho_B \approx 0.00373$  and  $0.0204 \text{ fm}^{-3}$ , respectively [1].

In addition to the QRPA results, we also show approximate results for the contribution of the collective mode obtained with the hydrodynamic sound velocity and Eq. (43) (dashed-dotted lines). At low temperatures, Eq. (43) is in perfect agreement with the QRPA result. This is a reassuring result since in many studies [4, 15–19] the contribution of the collective mode was calculated assuming the validity of the hydrodynamic approximation (long-wavelength limit). At higher temperatures, where the QRPA result starts to deviate considerably from Eq. (43), also our approximation to neglect temperature effects in the QRPA itself becomes questionable, as one can see from the increasing contribution of thermal quasiparticles.

Let also mention that at very low densities (such as  $\rho = 0.003 \text{ fm}^{-3}$ ), the sound velocity is close to that of an ideal Fermi gas,  $u \approx k_F/(\sqrt{3}m)$ , so that Eq. (43) is well approximated by  $c_{v,\text{coll}} \approx 2\sqrt{3}m^3 T^3/(15\rho)$ . While the discrepancy between this simple formula and Eq. (43) is less than 10% in the case of  $\rho = 0.003 \text{ fm}^{-3}$ , it is a factor of 3 in the case of  $\rho = 0.0184 \text{ fm}^{-3}$  where the sound velocity is considerably reduced by the attractive neutron-neutron interaction.

To assess the importance of the contribution of the collective mode to the specific heat of the inner crust, we show in Fig. 6 also the electron contribution (dotted lines), which is linear in temperature,

$$c_{v,e} = \frac{\mu_e^2 T}{3}. \quad (44)$$

The values of the electron chemical potentials  $\mu_e = 36.2$  and  $50.1 \text{ MeV}$  used in the upper and lower panel of Fig. 6, respectively, were obtained from the neutron and proton chemical potentials given in Ref. [1] and the relation  $\mu_e = \mu_n - \mu_p$  of  $\beta$ -equilibrium. One sees that, at not too low temperatures, the contribution of the collective mode is comparable to that of the electrons. In the case  $\rho = 0.003 \text{ fm}^{-3}$ , the contribution of the collective-mode even exceeds that of the electrons at  $T \gtrsim 150 \text{ keV}$ .

#### IV. CONCLUSION

In this work we used the QRPA to study collective excitations in a uniform superfluid neutron gas. We focused on low densities such as they are predicted in the inner crust of neutron stars. At these densities, the neutron pairing in the  $s$  wave is relatively strong. For the interaction, we used a Skyrme force in the  $ph$  channel and a separable interaction with a Gaussian form factor in the  $pp$  channel. We derived the QRPA density response by taking the small-amplitude limit of the TDHFB equations.

Since the HFB ground state breaks the global  $U(1)$  symmetry, a Goldstone mode, corresponding to phase oscillations of the superfluid gap, must exist. This

Bogoliubov-Anderson sound is actually a simple density wave, in other channels (e.g., spin modes) there are no ungapped modes. Since we treat the ph and pp residual interactions consistently with the HFB ground state, our QRPA density response automatically exhibits the Bogoliubov-Anderson sound with a linear dispersion relation  $\omega = uq$  at low momentum  $q$ . The speed of sound  $u$  coincides with the hydrodynamic one. However, as  $\omega$  approaches the pair-breaking threshold at  $\sim 2\Delta_{k_F}$ , substantial deviations from the linear dispersion relation are found: instead of crossing the threshold near  $q = 2\Delta_{k_F}/u$ , the dispersion relation of the collective mode bends, slowly approaches the threshold, and closely follows it, before it finally crosses it at a much higher  $q$  and enters into the two-quasiparticle continuum.

We also checked the quality of the Landau approximation to the residual interaction. We found that at low momenta ( $q \lesssim 1 \text{ fm}^{-1}$ ) the Landau approximation is sufficient to describe the collective mode. In this range of momenta, also the continuum of the response function is well described if one includes in addition to the  $l = 0$  Landau parameter  $F_0$  also the  $l = 1$  parameter  $F_1$ , as required to satisfy Galilean invariance in the case of an effective mass  $m^* \neq m$ . At higher momenta ( $q \gtrsim 1 \text{ fm}^{-1}$ ), the QRPA response function is not well reproduced by the Landau approximation. In this case, the inclusion of the parameter  $F_1$  in addition to  $F_0$  does not significantly improve the result. However, we note that in the case of a Skyrme interaction, the computation of the full QRPA response is almost as simple as the calculation within the Landau approximation, so that there is no good reason not to do the full calculation.

The existence of an ungapped collective mode has a strong effect on the heat capacity of the neutron gas. While quasiparticle excitations are exponentially suppressed at low temperature  $T \ll \Delta_{k_F}$  because of the gap, the collective mode can be excited at arbitrarily low temperatures and leads to a specific heat which is proportional to  $T^3$  at low  $T$ , increasing the neutron-gas contribution to the specific heat by several orders of magnitude in the temperature range relevant for neutron stars. Depending on density and temperature, the contribution of the collective mode to the specific heat of the inner neutron-star crust can be comparable to or even larger than that of the electrons.

As we have seen, in a uniform gas the QRPA response at low energies is well reproduced by simple hydrodynamics. However, in reality the neutron gas in the inner crust is not uniform, but it contains clusters having a higher density and consisting of neutrons and protons. These clusters form a Coulomb crystal. The clusters can also take the shape of cylinders or plates, in this case one speaks of “pasta phases”. The coupling between the collective mode of the neutron gas and the lattice phonons of the clusters is very important [17, 18]. As long as the coherence length of the Cooper pairs is less than the size of these structures, the hydrodynamic approach should remain a reasonable approximation. Work in this direction

TABLE II: Parameters of the Sly4 interaction for the case of pure neutron matter.

$s_0$ (MeV fm <sup>3</sup> )	-413.16
$s_1$ (MeV fm <sup>5</sup> )	654.29
$s_2$ (MeV fm <sup>5</sup> )	0
$s_3$ (MeV fm <sup>3+3<math>\alpha</math></sup> )	-4877.06
$\alpha$	1/6

has been done in Ref. [4] for the so-called “lasagne” phase and we plan to extend it to the other geometries (crystal, “spaghetti” phase). For an extension of the present study to the response of uniform matter with higher density, as it exists in the neutron star core, one has to include also the proton component and treat neutron pairing in the  $p$  wave.

For a complete description of cooling of neutron stars [49], the collective modes do not only play a role in the specific heat, but also in the heat conductivity. A discussion of these aspects, based on the long-wavelength approximation for the collective modes [17], can be found in Ref. [50]. Again, the coupling between the collective mode of the superfluid and the lattice phonons seems to be very important. Therefore, a unified description of the Bogoliubov-Anderson mode and the lattice phonons from a more microscopic perspective would be desirable.

### Acknowledgments

This work has been funded by the P2IO LabEx (ANR-10-LABX-0038) in the framework “Investissements d’Avenir” (ANR-11-IDEX-0003-01) managed by the French National Research Agency (ANR).

### Appendix A: Skyrme parameters

In spin-unpolarized pure neutron matter, the general Skyrme functional [21, 23, 24] takes the particularly simple form given in Eq. (1). The parameters  $s_i$  are related to the more common parameters  $t_i$  and  $x_i$  of Ref. [23] by

$$s_0 = t_0(1 - x_0), \quad (\text{A1a})$$

$$s_1 = t_1(1 - x_1), \quad (\text{A1b})$$

$$s_2 = t_2(1 + x_2), \quad (\text{A1c})$$

$$s_3 = t_3(1 - x_3). \quad (\text{A1d})$$

For the numerical values of the parameters  $t_i$ ,  $x_i$ , and  $\alpha$ , we use the SLy4 parametrization of Ref. [23]. For completeness, the parameters  $s_i$  and  $\alpha$  are listed in Table II. Decomposing the ph interaction matrix element Eq. (6)

according to Eq. (7), one obtains:

$$W_1(q) = s_0 + \frac{(\alpha + 2)(\alpha + 1)}{12} s_3 \rho^\alpha + \frac{s_1 - 3s_2}{4} q^2, \quad (\text{A2a})$$

$$W_2 = \frac{s_1 + 3s_2}{4}. \quad (\text{A2b})$$

### Appendix B: Matrix of response function

Below we give the explicit expressions for the 16 free quasiparticle response functions that form the matrix  $\Pi_{\mathbf{q}}^{(0)}$  in Eq. (25).

The  $\rho^+$  response:

$$\Pi_{\mathbf{k}_+, \mathbf{k}_-}^{\rho^+, h^+} = \frac{E_{\mathbf{k}_+} E_{\mathbf{k}_-} - \xi_{\mathbf{k}_+} \xi_{\mathbf{k}_-} + \Delta_{\mathbf{k}_+} \Delta_{\mathbf{k}_-}}{4E_{\mathbf{k}_+} E_{\mathbf{k}_-}} G_{\mathbf{k}, \mathbf{q}}^-(\omega), \quad (\text{B1a})$$

$$\Pi_{\mathbf{k}_+, \mathbf{k}_-}^{\rho^+, h^-} = -\frac{E_{\mathbf{k}_+} \xi_{\mathbf{k}_-} - \xi_{\mathbf{k}_+} E_{\mathbf{k}_-}}{4E_{\mathbf{k}_+} E_{\mathbf{k}_-}} G_{\mathbf{k}, \mathbf{q}}^+(\omega), \quad (\text{B1b})$$

$$\Pi_{\mathbf{k}_+, \mathbf{k}_-}^{\rho^+, \Delta^+} = -\frac{\xi_{\mathbf{k}_+} \Delta_{\mathbf{k}_-} + \Delta_{\mathbf{k}_+} \xi_{\mathbf{k}_-}}{4E_{\mathbf{k}_+} E_{\mathbf{k}_-}} G_{\mathbf{k}, \mathbf{q}}^-(\omega), \quad (\text{B1c})$$

$$\Pi_{\mathbf{k}_+, \mathbf{k}_-}^{\rho^+, \Delta^-} = -\frac{E_{\mathbf{k}_+} \Delta_{\mathbf{k}_-} + \Delta_{\mathbf{k}_+} E_{\mathbf{k}_-}}{4E_{\mathbf{k}_+} E_{\mathbf{k}_-}} G_{\mathbf{k}, \mathbf{q}}^+(\omega). \quad (\text{B1d})$$

The  $\rho^-$  response:

$$\Pi_{\mathbf{k}_+, \mathbf{k}_-}^{\rho^-, h^+} = -\frac{E_{\mathbf{k}_+} \xi_{\mathbf{k}_-} - \xi_{\mathbf{k}_+} E_{\mathbf{k}_-}}{4E_{\mathbf{k}_+} E_{\mathbf{k}_-}} G_{\mathbf{k}, \mathbf{q}}^+(\omega), \quad (\text{B1e})$$

$$\Pi_{\mathbf{k}_+, \mathbf{k}_-}^{\rho^-, h^-} = \frac{E_{\mathbf{k}_+} E_{\mathbf{k}_-} - \xi_{\mathbf{k}_+} \xi_{\mathbf{k}_-} - \Delta_{\mathbf{k}_+} \Delta_{\mathbf{k}_-}}{4E_{\mathbf{k}_+} E_{\mathbf{k}_-}} G_{\mathbf{k}, \mathbf{q}}^-(\omega), \quad (\text{B1f})$$

$$\Pi_{\mathbf{k}_+, \mathbf{k}_-}^{\rho^-, \Delta^+} = -\frac{E_{\mathbf{k}_+} \Delta_{\mathbf{k}_-} - \Delta_{\mathbf{k}_+} E_{\mathbf{k}_-}}{4E_{\mathbf{k}_+} E_{\mathbf{k}_-}} G_{\mathbf{k}, \mathbf{q}}^+(\omega), \quad (\text{B1g})$$

$$\Pi_{\mathbf{k}_+, \mathbf{k}_-}^{\rho^-, \Delta^-} = -\frac{\xi_{\mathbf{k}_+} \Delta_{\mathbf{k}_-} - \Delta_{\mathbf{k}_+} \xi_{\mathbf{k}_-}}{4E_{\mathbf{k}_+} E_{\mathbf{k}_-}} G_{\mathbf{k}, \mathbf{q}}^-(\omega). \quad (\text{B1h})$$

The  $\kappa^+$  response:

$$\Pi_{\mathbf{k}_+, \mathbf{k}_-}^{\kappa^+, h^+} = \frac{\xi_{\mathbf{k}_+} \Delta_{\mathbf{k}_-} + \Delta_{\mathbf{k}_+} \xi_{\mathbf{k}_-}}{4E_{\mathbf{k}_+} E_{\mathbf{k}_-}} G_{\mathbf{k}, \mathbf{q}}^-(\omega), \quad (\text{B1i})$$

$$\Pi_{\mathbf{k}_+, \mathbf{k}_-}^{\kappa^+, h^-} = \frac{E_{\mathbf{k}_+} \Delta_{\mathbf{k}_-} - \Delta_{\mathbf{k}_+} E_{\mathbf{k}_-}}{4E_{\mathbf{k}_+} E_{\mathbf{k}_-}} G_{\mathbf{k}, \mathbf{q}}^+(\omega), \quad (\text{B1j})$$

$$\Pi_{\mathbf{k}_+, \mathbf{k}_-}^{\kappa^+, \Delta^+} = -\frac{E_{\mathbf{k}_+} E_{\mathbf{k}_-} + \xi_{\mathbf{k}_+} \xi_{\mathbf{k}_-} - \Delta_{\mathbf{k}_+} \Delta_{\mathbf{k}_-}}{4E_{\mathbf{k}_+} E_{\mathbf{k}_-}} G_{\mathbf{k}, \mathbf{q}}^-(\omega), \quad (\text{B1k})$$

$$\Pi_{\mathbf{k}_+, \mathbf{k}_-}^{\kappa^+, \Delta^-} = -\frac{E_{\mathbf{k}_+} \xi_{\mathbf{k}_-} + \xi_{\mathbf{k}_+} E_{\mathbf{k}_-}}{4E_{\mathbf{k}_+} E_{\mathbf{k}_-}} G_{\mathbf{k}, \mathbf{q}}^+(\omega). \quad (\text{B1l})$$

The  $\kappa^-$  response:

$$\Pi_{\mathbf{k}_+, \mathbf{k}_-}^{\kappa^-, h^+} = \frac{E_{\mathbf{k}_+} \Delta_{\mathbf{k}_-} + \Delta_{\mathbf{k}_+} E_{\mathbf{k}_-}}{4E_{\mathbf{k}_+} E_{\mathbf{k}_-}} G_{\mathbf{k}, \mathbf{q}}^+(\omega), \quad (\text{B1m})$$

$$\Pi_{\mathbf{k}_+, \mathbf{k}_-}^{\kappa^-, h^-} = \frac{\xi_{\mathbf{k}_+} \Delta_{\mathbf{k}_-} - \Delta_{\mathbf{k}_+} \xi_{\mathbf{k}_-}}{4E_{\mathbf{k}_+} E_{\mathbf{k}_-}} G_{\mathbf{k}, \mathbf{q}}^-(\omega), \quad (\text{B1n})$$

$$\Pi_{\mathbf{k}_+, \mathbf{k}_-}^{\kappa^-, \Delta^+} = -\frac{E_{\mathbf{k}_+} \xi_{\mathbf{k}_-} + \xi_{\mathbf{k}_+} E_{\mathbf{k}_-}}{4E_{\mathbf{k}_+} E_{\mathbf{k}_-}} G_{\mathbf{k}, \mathbf{q}}^+(\omega), \quad (\text{B1o})$$

$$\Pi_{\mathbf{k}_+, \mathbf{k}_-}^{\kappa^-, \Delta^-} = -\frac{E_{\mathbf{k}_+} E_{\mathbf{k}_-} + \xi_{\mathbf{k}_+} \xi_{\mathbf{k}_-} + \Delta_{\mathbf{k}_+} \Delta_{\mathbf{k}_-}}{4E_{\mathbf{k}_+} E_{\mathbf{k}_-}} G_{\mathbf{k}, \mathbf{q}}^-(\omega). \quad (\text{B1p})$$

In the above expressions we have used the abbreviation

$$G_{\mathbf{k}, \mathbf{q}}^\pm(\omega) = \frac{1}{\omega - \Omega_{\mathbf{k}, \mathbf{q}} + i\eta} \pm \frac{1}{\omega + \Omega_{\mathbf{k}, \mathbf{q}} + i\eta}, \quad (\text{B2})$$

where  $\Omega_{\mathbf{k}, \mathbf{q}} = E_{\mathbf{k}_+} + E_{\mathbf{k}_-}$ .

The matrix  $\langle\langle \Pi_{\mathbf{q}}^{(0)} V \rangle\rangle$  used in Eq. (32) is defined as

$$\begin{aligned}
\langle\langle \Pi_{\mathbf{q}}^{(0)} V \rangle\rangle = & \\
W_1(q) & \begin{pmatrix} \langle\langle \Pi_{\mathbf{k}_+, \mathbf{k}_-}^{\rho^+, h^+} \rangle\rangle & 0 & 0 & 0 & 0 \\ \langle\langle k^2 \Pi_{\mathbf{k}_+, \mathbf{k}_-}^{\rho^+, h^+} \rangle\rangle & 0 & 0 & 0 & 0 \\ \langle\langle kz \Pi_{\mathbf{k}_+, \mathbf{k}_-}^{\rho^+, h^+} \rangle\rangle & 0 & 0 & 0 & 0 \\ \langle\langle F(k) \Pi_{\mathbf{k}_+, \mathbf{k}_-}^{\kappa^+, h^+} \rangle\rangle & 0 & 0 & 0 & 0 \\ \langle\langle F(k) \Pi_{\mathbf{k}_+, \mathbf{k}_-}^{\kappa^-, h^+} \rangle\rangle & 0 & 0 & 0 & 0 \end{pmatrix} + W_2 \begin{pmatrix} \langle\langle k^2 \Pi_{\mathbf{k}_+, \mathbf{k}_-}^{\rho^+, h^+} \rangle\rangle & \langle\langle \Pi_{\mathbf{k}_+, \mathbf{k}_-}^{\rho^+, h^+} \rangle\rangle & -2\langle\langle kz \Pi_{\mathbf{k}_+, \mathbf{k}_-}^{\rho^+, h^+} \rangle\rangle & 0 & 0 \\ \langle\langle k^4 \Pi_{\mathbf{k}_+, \mathbf{k}_-}^{\rho^+, h^+} \rangle\rangle & \langle\langle k^2 \Pi_{\mathbf{k}_+, \mathbf{k}_-}^{\rho^+, h^+} \rangle\rangle & -2\langle\langle k^3 z \Pi_{\mathbf{k}_+, \mathbf{k}_-}^{\rho^+, h^+} \rangle\rangle & 0 & 0 \\ \langle\langle k^3 z \Pi_{\mathbf{k}_+, \mathbf{k}_-}^{\rho^+, h^+} \rangle\rangle & \langle\langle kz \Pi_{\mathbf{k}_+, \mathbf{k}_-}^{\rho^+, h^+} \rangle\rangle & -2\langle\langle k^2 z^2 \Pi_{\mathbf{k}_+, \mathbf{k}_-}^{\rho^+, h^+} \rangle\rangle & 0 & 0 \\ \langle\langle F(k) k^2 \Pi_{\mathbf{k}_+, \mathbf{k}_-}^{\kappa^+, h^+} \rangle\rangle & \langle\langle F(k) \Pi_{\mathbf{k}_+, \mathbf{k}_-}^{\kappa^+, h^+} \rangle\rangle & -2\langle\langle F(k) kz \Pi_{\mathbf{k}_+, \mathbf{k}_-}^{\kappa^+, h^+} \rangle\rangle & 0 & 0 \\ \langle\langle F(k) k^2 \Pi_{\mathbf{k}_+, \mathbf{k}_-}^{\kappa^-, h^+} \rangle\rangle & \langle\langle F(k) \Pi_{\mathbf{k}_+, \mathbf{k}_-}^{\kappa^-, h^+} \rangle\rangle & -2\langle\langle F(k) kz \Pi_{\mathbf{k}_+, \mathbf{k}_-}^{\kappa^-, h^+} \rangle\rangle & 0 & 0 \end{pmatrix} \\
+ g & \begin{pmatrix} 0 & 0 & 0 & \langle\langle F(k) \Pi_{\mathbf{k}_+, \mathbf{k}_-}^{\rho^+, \Delta^+} \rangle\rangle & \langle\langle F(k) \Pi_{\mathbf{k}_+, \mathbf{k}_-}^{\rho^+, \Delta^-} \rangle\rangle \\ 0 & 0 & 0 & \langle\langle F(k) k^2 \Pi_{\mathbf{k}_+, \mathbf{k}_-}^{\rho^+, \Delta^+} \rangle\rangle & \langle\langle F(k) k^2 \Pi_{\mathbf{k}_+, \mathbf{k}_-}^{\rho^+, \Delta^-} \rangle\rangle \\ 0 & 0 & 0 & \langle\langle F^2(k) \Pi_{\mathbf{k}_+, \mathbf{k}_-}^{\kappa^+, \Delta^+} \rangle\rangle & \langle\langle F^2(k) \Pi_{\mathbf{k}_+, \mathbf{k}_-}^{\kappa^+, \Delta^-} \rangle\rangle \\ 0 & 0 & 0 & \langle\langle F^2(k) \Pi_{\mathbf{k}_+, \mathbf{k}_-}^{\kappa^-, \Delta^+} \rangle\rangle & \langle\langle F^2(k) \Pi_{\mathbf{k}_+, \mathbf{k}_-}^{\kappa^-, \Delta^-} \rangle\rangle \\ 0 & 0 & 0 & \langle\langle F^2(k) \Pi_{\mathbf{k}_+, \mathbf{k}_-}^{\kappa^-, \Delta^+} \rangle\rangle & \langle\langle F^2(k) \Pi_{\mathbf{k}_+, \mathbf{k}_-}^{\kappa^-, \Delta^-} \rangle\rangle \end{pmatrix}, \quad (\text{B3})
\end{aligned}$$

with  $z = \cos \angle(\mathbf{k}, \mathbf{q})$ .

### Appendix C: Numerical computation

In Appendix B we gave the equations needed to determine the QRPA response function. In practice, the summations over  $\mathbf{k}$  are integrals. In our numerical calculations we start by evaluating the imaginary parts of the matrix  $\langle\langle \Pi_{\mathbf{q}}^{(0)} V \rangle\rangle$ . According to Eqs. (B1) and (B3), each element of this matrix can be written in the form

$$\langle\langle \Pi_{\mathbf{q}}^{(0)}(\omega) V \rangle\rangle_{\alpha\beta} = \int \frac{d^3k}{(2\pi)^3} f_{\alpha\beta}(k, q, z) G_{\mathbf{k}, \mathbf{q}}^{\pm}(\omega). \quad (\text{C1})$$

Then the the imaginary part is given by :

$$\text{Im} \langle\langle \Pi_{\mathbf{q}}^{(0)}(\omega) V \rangle\rangle = \frac{1}{2\pi^2} \int_0^{z_{\max}} dz \sum_i \frac{k_i^2 f(k_i, q, z)}{\left| \frac{\partial \Omega_{\mathbf{k}, \mathbf{q}}}{\partial k} \right|_{k_i}}, \quad (\text{C2})$$

where  $\{k_i\}$  is the set of solutions of the equation  $\Omega_{\mathbf{k}, \mathbf{q}} = \omega$  for a given angle  $z$ , and  $z_{\max}$  is either 1 or the angle beyond which the equation  $\Omega_{\mathbf{k}, \mathbf{q}} = \omega$  does not have a solution any more. After the calculation of the imaginary part, we compute the real part with the help of a dispersion relation,

$$\begin{aligned}
\text{Re} \langle\langle \Pi_{\mathbf{q}}^{(0)}(\omega) V \rangle\rangle = & -\frac{1}{\pi} \int_0^{\infty} d\omega' \text{Im} \langle\langle \Pi_{\mathbf{q}}^{(0)}(\omega') V \rangle\rangle \\
& \times \left( \frac{1}{\omega - \omega'} \pm \frac{1}{\omega + \omega'} \right), \quad (\text{C3})
\end{aligned}$$

where the sign  $\pm$  is chosen according to the sign in  $G^{\pm}$  in Eq. (C1).

- 
- [1] J. Negele and D. Vautherin, Nucl. Phys. A **207**, 298 (1973).
  - [2] M. Fortin, F. Grill, J. Margueron, D. Page, and N. Sandulescu, Phys. Rev. C **82**, 065804 (2010).
  - [3] E. Khan, N. Sandulescu, and N. V. Giai, Phys. Rev. C **71**, 042801 (2005).
  - [4] L. Di Gallo, M. Oertel, and M. Urban, Phys. Rev. C **84**, 045801 (2011).
  - [5] C. García-Recio, J. Navarro, V. G. Nguyen, and L. Salcedo, Ann. Phys. (N.Y.) **214**, 293 (1992).
  - [6] A. Pastore, M. Martini, V. Buridon, D. Davesne, K. Benhaceur, and J. Meyer, Phys. Rev. C **86**, 044308 (2012).
  - [7] J. Margueron, I. Vidaña, and I. Bombaci, Phys. Rev. C **68**, 055806 (2003).
  - [8] J. Keller and A. Sedrakian, Phys. Rev. C **87**, 045804 (2013).
  - [9] M. Baldo and C. Ducoin, Phys. Rev. C **84**, 035806 (2011).
  - [10] S. Bogner, R. Furnstahl, S. Ramanan, and A. Schwenk, Nucl. Phys. A **784**, 79 (2007).
  - [11] N. Bogoliubov, V. Tolmachev, and D. Shirkov, *A New Method in the Theory of Superconductivity* (Consultants Bureau, New York, 1959).
  - [12] P. W. Anderson, Phys. Rev. **112**, 1900 (1958).
  - [13] J. Goldstone, A. Salam, and S. Weinberg, Phys. Rev. **127**, 965 (1962).
  - [14] R. Combescot, M. Y. Kagan, and S. Stringari, Phys. Rev. A **74**, 042717 (2006).
  - [15] D. N. Aguilera, V. Cirigliano, J. A. Pons, S. Reddy, and R. Sharma, Phys. Rev. Lett. **102**, 091101 (2009).
  - [16] N. Chamel, S. Goriely, J. M. Pearson, and M. Onsi, Phys. Rev. C **81**, 045804 (2010).
  - [17] V. Cirigliano, S. Reddy, and R. Sharma, Phys. Rev. C **84**, 045809 (2011).
  - [18] N. Chamel, D. Page, and S. Reddy, Phys. Rev. C **87**,

- 035803 (2013).
- [19] D. Kobayakov and C. J. Pethick, *Phys. Rev. C* **87**, 055803 (2013).
- [20] M. M. Forbes and R. Sharma, *Phys. Rev. A* **90**, 043638 (2014).
- [21] D. Vautherin and D. M. Brink, *Phys. Rev. C* **5**, 626 (1972).
- [22] E. Chabanat, P. Bonche, P. Haensel, J. Meyer, and R. Schaeffer, *Nucl. Phys. A* **627**, 710 (1997).
- [23] E. Chabanat, P. Bonche, P. Haensel, J. Meyer, and R. Schaeffer, *Nucl. Phys. A* **635**, 231 (1998).
- [24] Y. Engel, D. Brink, K. Goeke, S. Krieger, and D. Vautherin, *Nucl. Phys. A* **249**, 215 (1975).
- [25] J. Navarro, E. S. Hernández, and D. Vautherin, *Phys. Rev. C* **60**, 045801 (1999).
- [26] J. Bardeen, L. N. Cooper, and J. R. Schrieffer, *Phys. Rev.* **108**, 1175 (1957).
- [27] R. Tamagaki, *Prog. Theor. Phys.* **44**, 905 (1970).
- [28] E. Khan, N. Sandulescu, M. Grasso, and N. Van Giai, *Phys. Rev. C* **66**, 024309 (2002).
- [29] S. Ramanan and M. Urban, *Phys. Rev. C* **88**, 054315 (2013).
- [30] P. Ring and P. Schuck, *The Nuclear Many-Body Problem* (Springer, Berlin, 1980).
- [31] A. Sedrakian and J. Keller, *Phys. Rev. C* **81**, 045806 (2010).
- [32] S. Weinberg, *The Quantum Theory of Fields: Volume 2, Modern Applications*, *Quantum Theory of Fields* (Cambridge University Press, Cambridge, 2005).
- [33] P. Nozières, *Theory of interacting Fermi systems* (Benjamin, New York, 1964).
- [34] A. Legget, *Physical Review* **147**, 119 (1966).
- [35] C. Menotti, P. Pedri, and S. Stringari, *Phys. Rev. Lett.* **89**, 250402 (2002).
- [36] M. Grasso, E. Khan, and M. Urban, *Phys. Rev. A* **72**, 043617 (2005).
- [37] F. Douchin and P. Haensel, *Phys. Lett. B* **485**, 107 (2000).
- [38] K. Hebeler, A. Schwenk, and B. Friman, *Physics Letters B* **648**, 176 (2007).
- [39] D. J. Dean and M. Hjorth-Jensen, *Rev. Mod. Phys.* **75**, 607 (2003).
- [40] N. Chamel and P. Haensel, *Living Reviews in Relativity* **11**, 10 (2008).
- [41] L. P. Gor'kov and T. K. Melik-Barkhudarov, *Soviet Physics JETP* **13**, 1018 (1961).
- [42] A. Gezerlis and J. Carlson, *Phys. Rev. C* **77**, 032801 (2008).
- [43] A. Gezerlis and J. Carlson, *Phys. Rev. C* **81**, 025803 (2010).
- [44] M. Tinkham, *Introduction to Superconductivity* (McGraw-Hill, New York, 1975).
- [45] A. Fetter and J. Walecka, *Quantum Theory of Many-particle Systems* (McGraw-Hill, New York, 1971).
- [46] Y. Nambu, *Phys. Rev.* **117**, 648 (1960).
- [47] P. Debye, *Ann. Phys. (Leipzig)* **344**, 789 (1912).
- [48] N. Ashcroft and N. Mermin, *Solid state physics* (Saunders College, Fort Worth, 1976).
- [49] D. Page and S. Reddy, *Phys. Rev. Lett.* **111**, 241102 (2013).
- [50] D. Page and S. Reddy, *ArXiv e-prints* (2012), arXiv:1201.5602 [nucl-th] .